

A surfactant-assisted probe for the chromo-fluorogenic selective recognition of GSH in water

Alessandro Agostini, Inmaculada Campos, Michele Milani, Sameh Elsayed, Lluís Pascual, Ramón Martínez-Máñez, Maurizio Licchelli and Félix Sancenón

Chemicals

The chemicals cetyltrimethylammonium bromide (CTAB), 4-(2-hydroxyethyl)-1-piperazineethanesulfonic acid (HEPES), acetophenone, triethylorthoformate, methyl iodide, magnesium, perchloric acid, tetraphenylphosphonium tetrafluoroborate, 4-hydroxybenzaldehyde, GSH and selected amino acids (Cys, Hcy, Ala, Arg, Asn, Asp, Glu, Gln, Gly, His, Ile, Leu, Lys, Met, Phe, Pro, Ser, Thr, Trp, Tyr, Val) were provided by Sigma-Aldrich. Analytical-grade solvents were from Scharlab (Barcelona, Spain). All reagents were used as received.

General Techniques

Fluorescence spectroscopy was carried out with a Jasco Spectrofluorometer FP-8500. 1D and 2D NMR spectra were recorded on a Bruker AVANCE III 400 MHz Spectrometer, where ^1H NMR spectra were recorded at 400 MHz at 298 K, while ^{13}C NMR spectra were recorded at 100 MHz at 298 K. The NMR samples were dissolved in deuterated solvents purchased from Cambridge Isotope Labs or Sigma-Aldrich, and TMS or the residual solvent were used as internal standard. Electron impact ionization mass spectrometry (MS-EI) was performed on a Thermo Finnigan MAT SSQ710 single stage quadropole instrument. Matrix-assisted laser-desorption/ionization mass spectrometry was performed on a Bruker Autoflex III Smartbeam mass spectrometer, utilizing a 2,5-dihydroxybenzoic acid (DHB) matrix.

Deprotonation of 5 in non aqueous solvents

An acetonitrile solution of **1** (2.5×10^{-5} M) was titrated with *N,N,N',N'*-tetramethyl-1,8-diaminonaphthalene (*proton sponge*, strong non-nucleophilic base), and the chromogenic changes were monitored. Spectra taken during the titration experiment and the corresponding titration profile are reported in figure SI-1. Chemodosimeter **1** displays a strong absorption in the 350-700 nm range of the electronic spectrum (maxima at 410 and 500 nm) that is responsible for the observed red-orange colour. Addition of increasing quantities of the non-nucleophilic base induced a progressive red-shift of the absorption bands with an intensity increase in the 500-700 nm interval (maximum at 549 nm). The titration profile determined by plotting molar absorbance at 550 nm vs equivalent ratio (mol of *proton sponge*/mol of **1**) suggest an 1:1 stoichiometry for the process involving **1** and the base. The spectral changes were ascribed to the deprotonation of phenol moiety of **1** that yielded the quinone derivative **2** (see Scheme 1 in the manuscript). The presence of an isosbestic point (508 nm) supports the coexistence of only two species (i.e. chemodosimeter **1** and quinone **2**) at the equilibrium. Non-linear least-square treatment of spectral data by Hyperquad software package¹ provided a $\log K = 7.10 \pm 0.06$ for the deprotonation equilibrium.

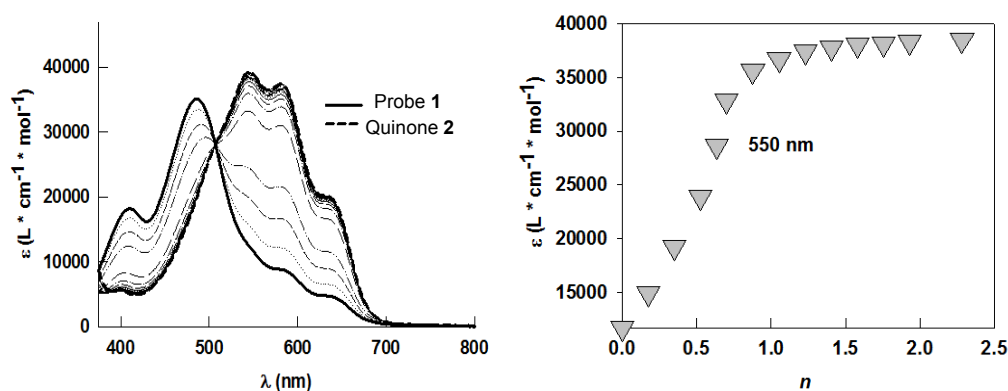


Figure SI-1. Family of spectra taken in the course of the titration of an acetonitrile solution of **1** (2.5×10^{-5} M) with a standard solution of proton sponge (left) and the corresponding titration profile ($n = \text{equiv proton sponge/equiv } \mathbf{1}$) determined at 550 nm (right).

¹ P. Gans, A. Sabatini and A. Vacca, *Talanta*, **1996**, *43*, 1739; <http://www.hyperquad.co.uk/index.htm>

The formation of the quinone form **2**, upon deprotonation of chemodosimeter **1** with 1,8-diazabicyclo[5.4.0]undec-7-ene (DBU, non-nucleophilic base) was also assessed by ¹H- and ¹³C-NMR measurements in DMSO-D6. ¹H-NMR spectrum of the product obtained upon DBU-induced deprotonation of chemodosimeter **1** are reported in figure SI-2, whereas the ¹³C-NMR spectrum is depicted in figure SI-3.

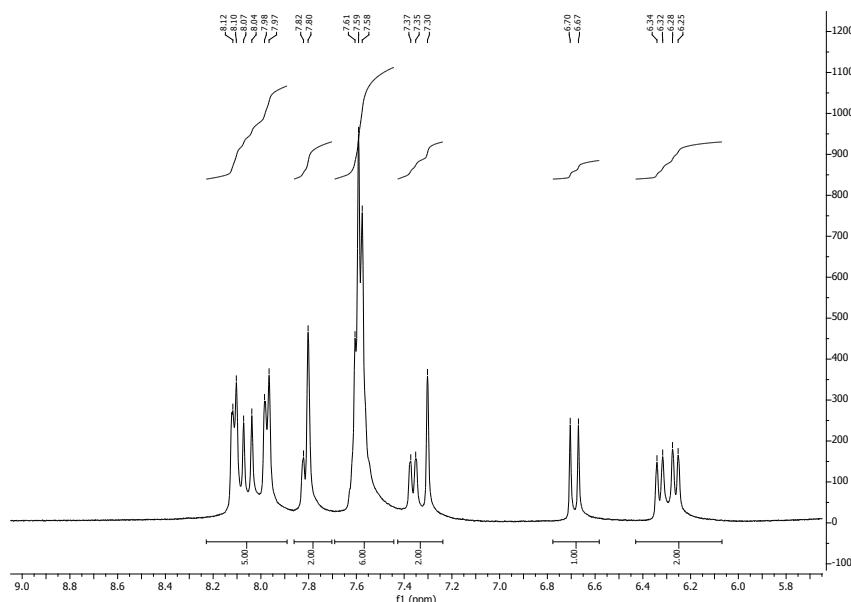


Figure SI-2. ¹H-NMR spectra of **2** (obtained upon addition of DBU to chemodosimeter **1**) in DMSO-D6.

As could be seen in figure SI-2, the most remarkable features of the ¹H-NMR spectra of quinone **2**, when compared with the spectra of chemodosimeter **1**, are the significant upfield shifts (from 8.7 and 7.4 ppm in **1** to 8.1 and 6.7 ppm in **2**) of the signals of the double bond protons (H_a and H_b , see scheme 1 in the manuscript) together with a reduction of the coupling constant (from 16 to 12 Hz). Also, the hydroxyl proton signal centred at 10.8 ppm disappeared upon addition of base.

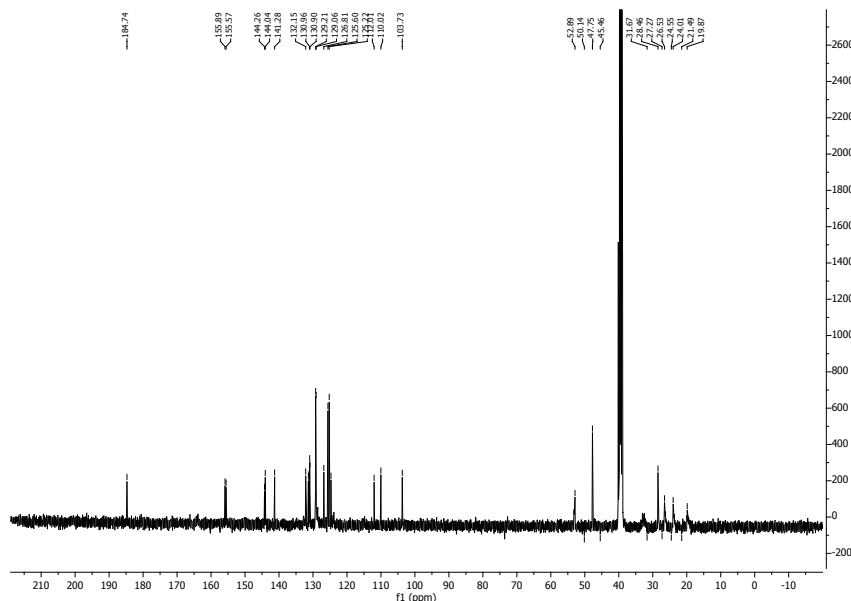


Figure SI-3. ¹³C-NMR spectra of **2** (obtained upon addition of DBU to chemodosimeter **1**) in DMSO-D6.

Formation of **6** in micelles proved by UV-vis measurements

In order to assess the formation of the quinone form **2** (see Scheme 1 in the manuscript) when chemodosimeter **1** was dissolved in HEPES (30 mM, pH 7.5)-CTAB (20 mM) solutions further UV-visible measurements were carried out. As described above, addition of one equivalent of proton sponge (as well as DBU) to acetonitrile solutions of **1** (1.0×10^{-5} M) induced a change in color from orange-red to blue due to the appearance of intense absorption bands in the 500-700 nm range. The change in color and the new bands were ascribed to the quinone **2** generated by the deprotonation reaction of the phenol moiety of chemodosimeter **1** (see figure SI-4).

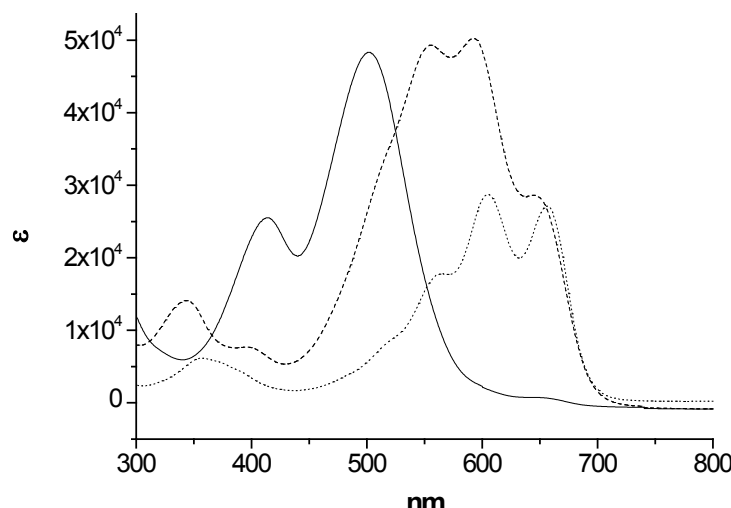


Figure SI-4. UV-visible spectra of chemodosimeter **1** (1.0×10^{-5} M) in acetonitrile (filled line), **1** upon addition of one equivalent of DBU (dashed line) and **1** (2.5×10^{-5} M) dissolved in HEPES-CTAB solution (dotted line).

Figure SI-4 also shows the UV-visible spectrum of chemodosimeter **1** (2.5×10^{-5} M) in HEPES (30 mM, pH 7.5)-CTAB (20 mM) solution. The same intense absorption bands (in the 500-700 nm interval) obtained upon treatment of acetonitrile solutions of **1** with DBU were observed in aqueous environment. This suggests that inclusion of chemodosimeter **1** into the hydrophobic environment in the inner of the CTAB micelles induced the deprotonation of the phenol moiety with the subsequent stabilization of the less polar quinone **2**.

Mechanism of the chromo-fluorogenic response in the presence of GSH

The mechanism of the chromo-fluorogenic response was studied by means of NMR measurements with quinone **2** (generated upon addition of DBU or *proton sponge* to chemodosimeter **1**) and GSH in DMSO-D6. The high complexity of the spectra obtained upon reaction of GSH with quinone **2** suggested us the use of a simple thiol derivative (such as 2-mercaptoethanol) in order to determine the mechanism of the observed response. ¹H (figure SI-5), COSY (figure SI-6), DEPT (figure SI-7), sel-TOCSY (figure SI-8) and HSQC (figure SI-9) NMR measurements were carried out, in order to characterize the addition product of 2-mercaptoethanol to **2**.

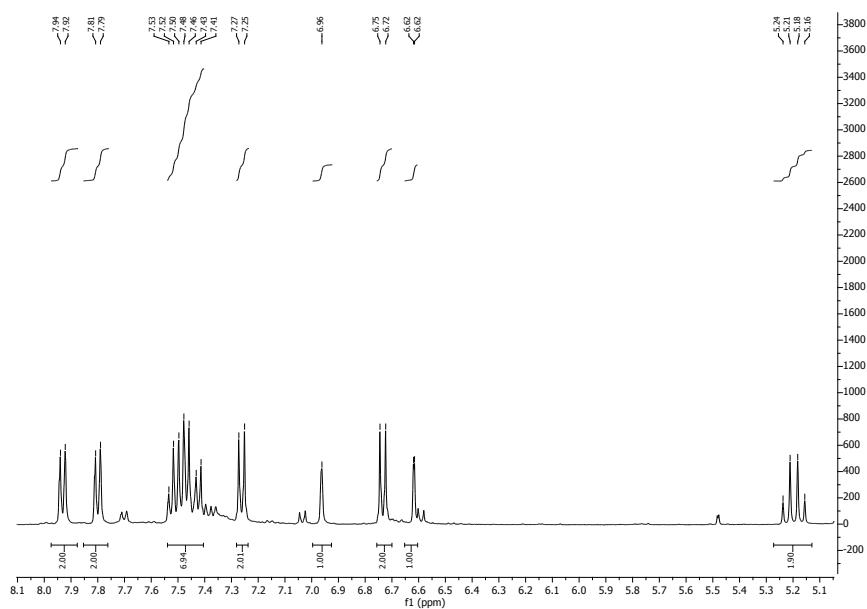


Figure SI-5. Aromatic part of the ¹H-NMR spectra of the addition product of 2-mercaptopropanoic acid to **2** in DMSO-D6.

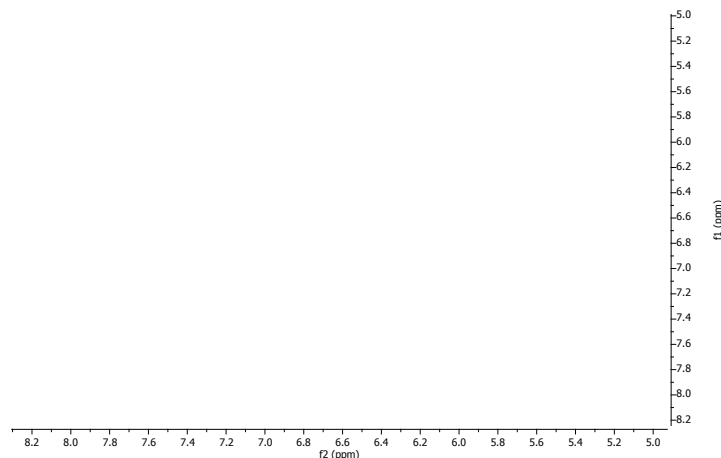


Figure SI-6. COSY spectra of the addition product of 2-mercaptopropanoic acid to **2** in DMSO-D6.

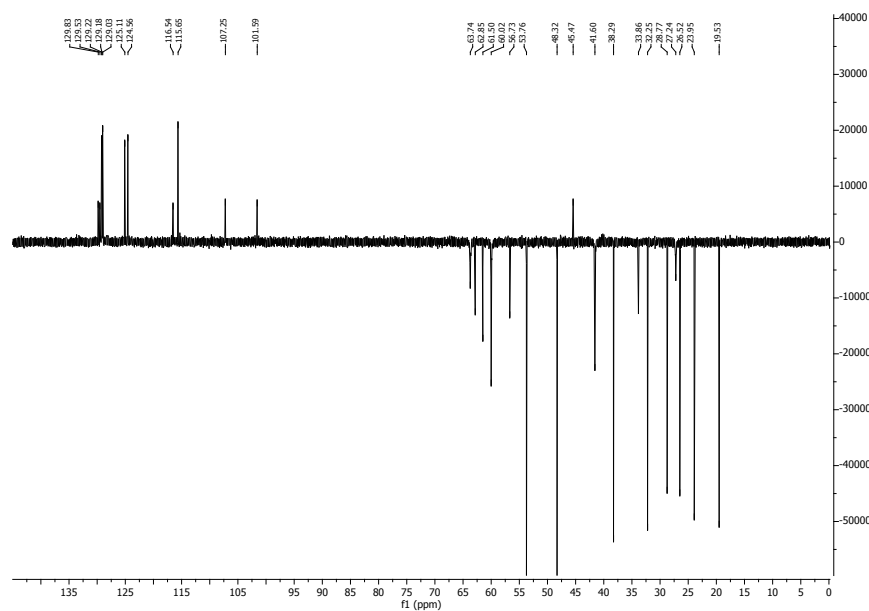


Figure SI-7. DEPT spectra of the addition product of 2-mercaptopropanoic acid to **2** in DMSO-D6.

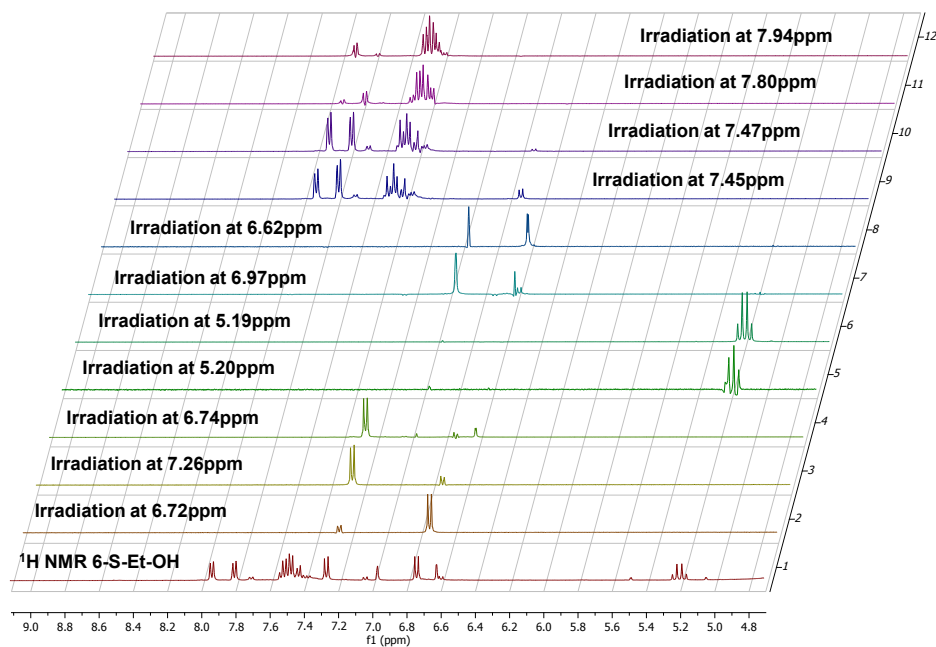


Figure SI-8. sel-TOCSY spectra of the addition product of 2-mercaptopropanoic acid to **2** in DMSO-D6.

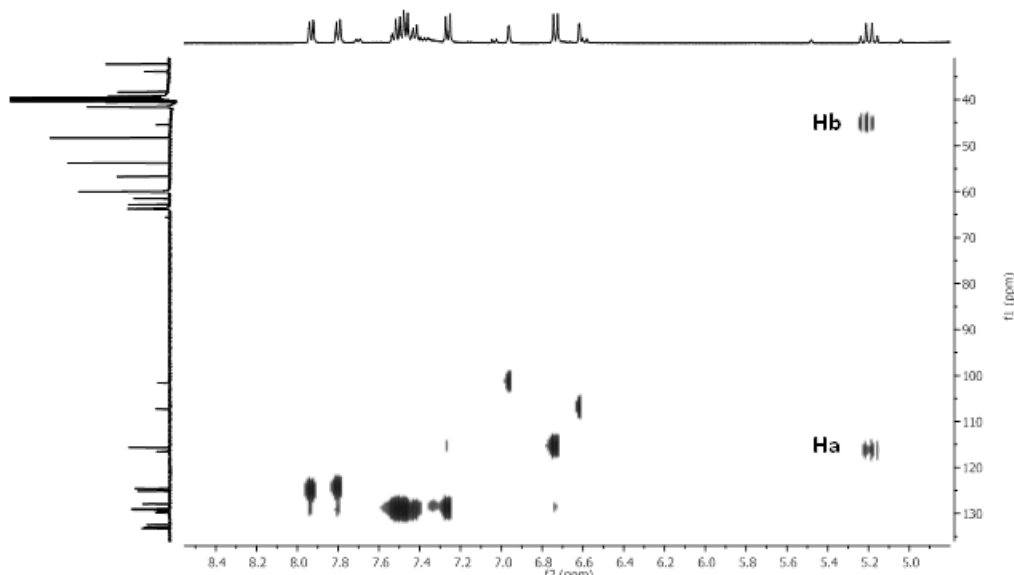


Figure SI-9. HSQC spectra of the addition product of 2-mercaptoproethanol to **2** in DMSO-D6.

HSQC experiment resulted the most remarkable of all the NMR measurements carried out to elucidate the chromo-fluorogenic mechanism and to identify the final product of the reaction involving quinone **2** and 2-mercaptoproethanol. HSQC spectra (figure SI-9) of the reaction product clearly indicated the existence of a correlation between H_b proton (see figure SI-9 and figure SI-10) and a benzylic carbon (at ca. 45 ppm) and also between H_a proton and an olefinic carbon (at ca. 116 ppm). These correlations clearly pointed to a thiol 1,6-conjugated addition that yielded product **3** (see also figure SI-10). Moreover, we were able to isolate the final product of the reaction between **2** and GSH. HRMS-ESI measurements indicated the formation of **3** with an m/z of 657.2152 (657.2145 calculated for $\text{C}_{35}\text{H}_{35}\text{N}_3\text{O}_8\text{S}$).

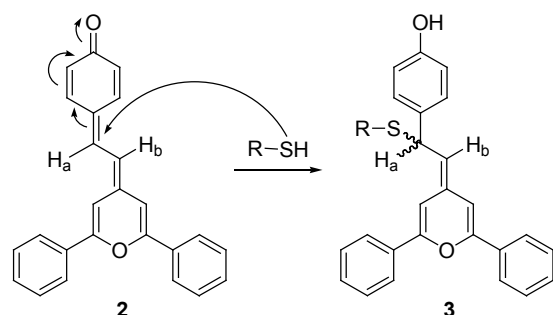


Figure SI-10. Mechanism of the 1,6-conjugated addition of thiol-containing bio-molecules to chemodosimeter **2**.

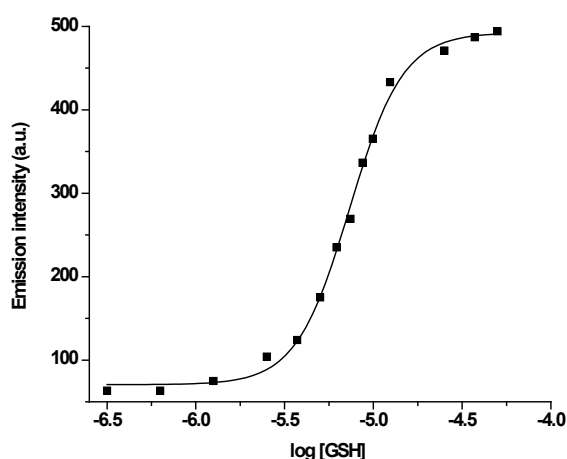


Figure SI-11. Changes in the emission band centered at 485 nm (excitation at 350 nm) of HEPES (30 mM, pH 7.5)-CTAB (20 mM) solutions of **2** (2.5×10^{-5} M) upon addition of increasing quantities of GSH.

Determination of GSH limit of detection

Changes in the emission band centred at 485 nm (excitation at 350 nm) of HEPES-CTAB (20 mM) solutions of **2** (2.5×10^{-5} M) were monitored upon addition of increasing amounts of GSH. This addition induced a progressive enhancement of the emission band at 485 nm. From the calibration curve a detection limit for GSH of 1.0 μ M was calculated (see figure SI-11).

Determination of GSH in plasma

GSH was determined in artificial human plasma by a standard addition method.² The artificial plasma was prepared according to a well-established method. Then the plasma was doped with conventional quantity of biothiols (Cys: 178.4 μ M; Hcy: 5.9 μ M and GSH: 6.3 μ M).³ Following this 20 μ L of the obtained plasma were added to 2.7 mL of chemodosimeter **2** (2.5×10^{-4} M) in HEPES-CTAB (20 mM). A standard addition method was carried out by measuring the emission of the solution of chemodosimeter **2** in the presence of increasing concentrations of GSH (2.5×10^{-6} to 1.75×10^{-5} M range). The determined GSH concentration in artificial plasma was 5.92 μ M, with a calculated recovery of 94.0%. The recovery clearly indicated that GSH was determined without any interference from Cys and Hcy.

X-ray crystallographic study

Diffraction data for a blue crystal (dimensions of about 0.50 x 0.42 x 0.30 mm) of **1**(NO₃) have been collected at ambient temperature by means of an Enraf-Nonius CAD4 four circle diffractometer equipped with a punctual detector (scintillation counter). **1**(BF₄) forms only small single crystals and diffraction data for a blue crystal (dimensions of about 0.15 x 0.12 x 0.08 mm) have been collected at ambient temperature by means of a Bruker-Axs CCD-based diffractometer. Both diffractometers work with graphite-monochromatized MoK α X-radiation ($\lambda = 0.71073$ Å). Crystal data for the two molecular complexes are shown in Table SI-1. Data reductions (including intensity integration, background, Lorentz and polarization corrections) for intensities collected with the conventional diffractometer were performed with the WinGX package;⁴ absorption correction was not applied to the data. Frames collected by the CCD-based system were processed with the SAINT software⁵ and intensities were corrected for Lorentz and polarization effects; absorption effects were empirically evaluated by the SADABS software⁶ and absorption correction was applied to the data (min./max. transmission factors were 0.806/0.992).

Table SI-1. Crystal data for investigated crystals.

	1 (NO ₃)	1 (BF ₄)
Formula	C ₂₅ H ₁₉ O ₅ N	C ₂₅ H ₁₉ O ₂ F ₄ B
<i>M</i>	413.41	438.21
Crystal system	Triclinic	Triclinic
Space group	<i>P</i> -1 (no. 2)	<i>P</i> -1 (no. 2)
<i>a</i> [Å]	8.846(2)	9.458(5)
<i>b</i> [Å]	10.208(3)	10.250(5)
<i>c</i> [Å]	12.644(3)	11.558(5)
α [°]	69.56(2)	83.424(5)
β [°]	84.07(2)	76.519(5)
γ [°]	73.221(19)	77.504(5)
<i>V</i> [Å ³]	1024.3(4)	1061.4(9)
<i>Z</i>	2	2
Temperature (K)	293	293
ρ_{calcd} [g cm ⁻³]	1.340	1.371
μ MoK α [mm ⁻¹]	0.094	0.109
Scan type	Ω scans	Ω scans
θ range [°]	2 – 25	2 – 25
Measured reflections	3795	11021
Unique reflections	3606	3779
<i>R</i> _{int}	0.0295	0.0319
Strong data [$I_O > 2\sigma(I_O)$]	2253	2242
Refined parameters	280	319
<i>RI</i> , <i>wR2</i> (strong data)	0.0849, 0.1377	0.0594, 0.0982
<i>RI</i> , <i>wR2</i> (all data)	0.1573, 0.1930	0.1577, 0.1941
GOF	1.130	1.021
Max/min residuals [eÅ ⁻³]	0.387 / -0.315	0.224 / -0.216

² M. R. C. Marques, R. Loebenberg, M. Almukainzi, *Dissolut. Technol.*, **2011**, 18, 15-28.

³ (a) J. F. Salazar, H. Schorr, W. Herrmann, B. Herbeth, G. Siest, P. Leroy, *J. of Chromatogr. Sci.*, **1999**, 37, 469-476. (b) T. D. Nolin, M. E. McMenamin, J. Himmelfarba, *J. Chromatogr. B Analyt. Technol. Biomed. Life. Sci.*, **2007**, 852, 554.

⁴ L.J. Farrugia, *J. Appl. Crystallogr.* **1999**, 32, 837-838.

⁵ Bruker. SAINT Software Reference Manual. Version 6. Bruker AXS Inc., Madison, Wisconsin, USA, **2003**.

⁶ G.M. Sheldrick. SADABS Siemens Area Detector Absorption Correction Program. University of Göttingen, Göttingen, Germany, **1996**.

Both crystal structures were solved by direct methods (SIR 97)⁷ and refined by full-matrix least-square procedures on F^2 using all reflections (SHELXL 97).⁸ Anisotropic displacement parameters were refined for all non-hydrogen atoms. Hydrogen atoms were placed at calculated positions with the appropriate AFIX instructions and refined using a riding model. CCDC 922786 and 922787 contain the supplementary crystallographic data for this paper. These data can be obtained free of charge via www.ccdc.cam.ac.uk/conts/retrieving.html (or from the Cambridge Crystallographic Data Centre, 12 Union Road, Cambridge CB21EZ, UK; fax: (+44) 1223-336-033; or e-mail: deposit@ccdc.cam.ac.uk).

The compound **1**(NO₃) crystallizes in the triclinic space group *P*-1 and the asymmetric unit is composed by one **1** ion and one NO₃⁻ counterion. ORTEP view of **1**(NO₃) is reported in figure SI-12. Pyrylium ring is coplanar with the hydroxystyryl group and one phenyl ring: the relative dihedral angle are 3.90° and 0.96°. The remaining phenyl ring forms a dihedral angle respect with the pyrylium group of 22.81°.

The flat aromatic groups favour the creation of face-to-face π -interactions. The π -stacked molecules form column having a zig-zag style show in figure SI-13. The shortest centroid-centroid distances occur between the pyrylium ring and the phenolic ring of an overlying **1** ion. Longer distances occur between pyrylium ring and the phenyl ring of an underlying **1** ion. The not-coplanar phenyl ring is not involved in supramolecular π -interactions.

The hydroxyl group acts as H-donor towards the nitrate counterion. The bifurcated O-H \cdots O H-bond involves as H-acceptor two O atoms of the same NO₃ group. The remaining O_{nitrate} atom profits of three very weak C-H \cdots O H-bonds having as H-donor species two CH groups of the aromatic rings and a CH of the olefinic C=C group. The H-bond motif originates the supramolecular dimer shown in figure SI-14. Geometrical features of the H-bond are reported in table SI-2. tables SI-3, SI-4 and SI-5 showed selected distances and angles for **1**(NO₃).

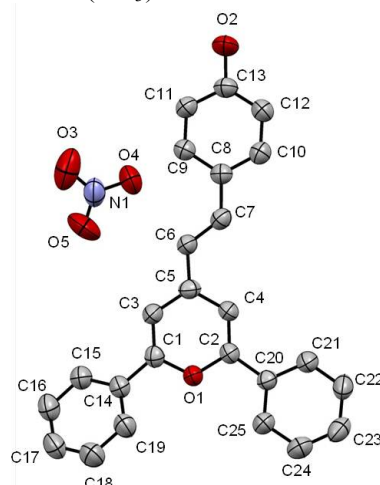


Figure SI-12. ORTEP view of the complex **1**(NO₃) (ellipsoids are drawn at the 50% probability level).

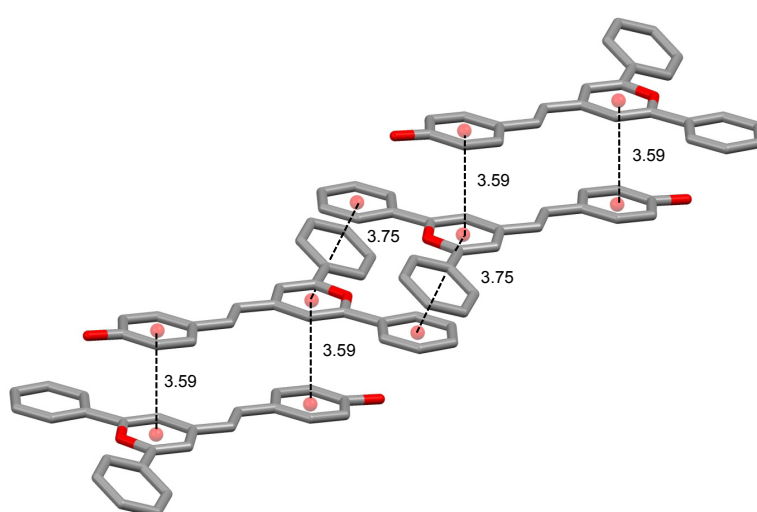


Figure SI-13. A simplified view of the π -stacked **1**(NO₃)

⁷ A. Altomare, M.C. Burla, M. Camalli, G.L. Cascarano, C. Giacovazzo, A. Guagliardi, A.G.G. Moliterni, G. Polidori, R. Spagna, *J. Appl. Crystallogr.* **1999**, *32*, 115-119

⁸ G.M. Sheldrick, *Acta Crystallogr.* **2008**, *A64*, 112-122.

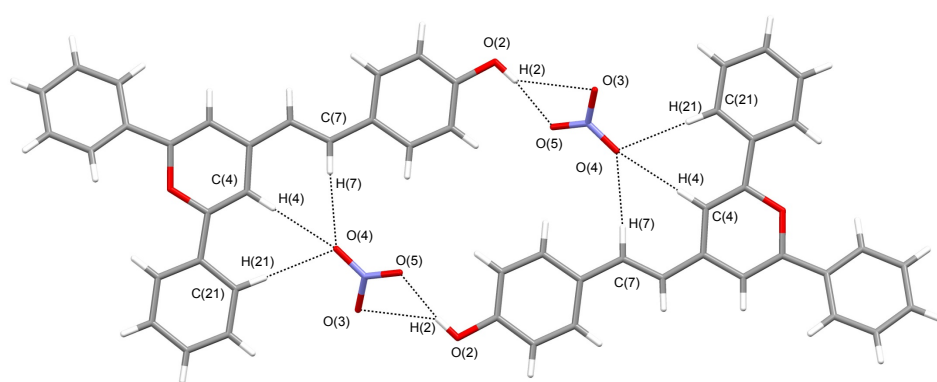


Figure SI-14. A simplified view of the H-bond-dimer **1**(NO₃)

Table SI-2. Geometrical features of hydrogen bonds distance in **1**(NO₃)

Donor group (D)	D···A (Å)	H···A (Å)	D-H···A (°)	Acceptor atom (A)
O(2)-H(2O)	3.191(1)	2.511(1)	141.12(1)	O(3) _{NO3-}
O(2)-H(2O)	2.769(1)	1.986(1)	159.43(1)	O(5) _{NO3-}
C(21)-H(21C)	3.777(1)	3.016(1)	158.85(1)	O(4) _{NO3-}
C(4)-H(4C)	3.300(1)	2.405(1)	161.46(1)	O(4) _{NO3-}
C(7)-H(7C)	3.375(1)	2.479(1)	161.90(1)	O(4) _{NO3-}

Table SI-3. π-π bonds distance (Å) for **1**(NO₃)

donor (D)	D···A
C(5)-C(8)	3.564
C(4)-C(8)	3.480
C(4)-C(9)	3.564
C(2)-C(11)	3.568
O(1)-C(13)	3.638
C(1)-C(12)	3.659
C(3)-C(10)	3.627
C(7)-C(7)	3.377
C(7)-C(6)	3.575
C(1)-C(23)	3.397
C(9)-C(9)	3.310
O(1)-C(24)	3.606
O(1)-C(20)	3.676
O(1)-C(25)	3.582
C(2)-C(25)	3.446
O(2)-C(21)	3.766
C(1)-C(22)	3.680
C(2)-C(20)	3.842
C(4)-C(25)	3.822
C(5)-C(24)	3.767
C(3)-C(23)	3.665
C(24)-C(24)	3.367
Centroid O(1)-C(5)—centroid C(8)-C(13)	3.594
Centroid O(1)-C(5)—centroid C(20)-C(25)	3.753
Centroid O(6)-C(7)—centroid C(6)-C(7)	3.575

Table SI-4. Distances bond (Å) for **1**(NO₃)

C1	C3	1.361(5)
C1	O1	1.362(4)
C1	C14	1.458(5)
C2	C4	1.349(5)
C2	O1	1.354(4)

C2	C20	1.466(5)
C3	C5	1.406(5)
C3	H3	0.9300
C4	C5	1.413(5)
C4	H4	0.9300
C5	C6	1.429(5)
C6	C7	1.344(5)
C6	H6	0.9300
C7	C8	1.448(5)
C7	H7	0.9300
C8	C9	1.396(5)
C8	C10	1.398(5)
C9	C11	1.376(5)
C9	H9	0.9300
C10	C12	1.372(6)
C10	H10	0.9300
C11	C13	1.392(6)
C11	H11	0.9300
C12	C13	1.375(6)
C12	H12	0.9300
C13	O2	1.357(5)
C14	C19	1.386(6)
C14	C15	1.390(6)
C15	C16	1.377(6)
C15	H15	0.9300
C16	C17	1.374(7)
C16	H16	0.9300
C17	C18	1.363(7)
C17	H17	0.9300
C18	C19	1.384(6)
C18	H18	0.9300
C19	H19	0.9300
C20	C25	1.387(5)
C20	C21	1.392(6)
C21	C22	1.385(6)
C21	H21	0.9300
C22	C23	1.367(6)
C22	H22	0.9300
C23	C24	1.368(6)
C23	H23	0.9300
C24	C25	1.383(6)
C24	H24	0.9300
C25	H25	0.9300
O2	H2O	0.8200
N1	O4	1.208(5)
N1	O5	1.207(6)
N1	O3	1.243(6)

Table SI-5. Angles **1**(NO₃)

C3	C1	O1	119.7(4)
C3	C1	C14	128.2(4)
O1	C1	C14	112.1(3)
C4	C2	O1	120.0(4)
C4	C2	C20	127.4(4)
O1	C2	C20	112.6(3)
C1	C3	C5	121.2(4)
C1	C3	H3	119.4
C5	C3	H3	119.4
C2	C4	C5	121.5(4)
C2	C4	H4	119.2

C5	C4	H4	119.2
C3	C5	C4	116.2(4)
C3	C5	C6	120.6(4)
C4	C5	C6	123.2(4)
C7	C6	C5	124.1(4)
C7	C6	H6	117.9
C5	C6	H6	117.9
C6	C7	C8	127.7(4)
C6	C7	H7	116.1
C8	C7	H7	116.1
C9	C8	C10	117.5(4)
C9	C8	C7	123.3(4)
C10	C8	C7	119.2(4)
C11	C9	C8	121.2(4)
C11	C9	H9	119.4
C8	C9	H9	119.4
C12	C10	C8	121.9(4)
C12	C10	H10	119.1
C8	C10	H10	119.1
C9	C11	C13	119.7(4)
C9	C11	H11	120.1
C13	C11	H11	120.1
C10	C12	C13	119.6(4)
C10	C12	H12	120.2
C13	C12	H12	120.2
O2	C13	C12	123.3(4)
O2	C13	C11	116.5(4)
C12	C13	C11	120.2(4)
C19	C14	C15	119.0(4)
C19	C14	C1	120.9(4)
C15	C14	C1	120.0(4)
C16	C15	C14	120.1(4)
C16	C15	H15	119.9
C14	C15	H15	119.9
C17	C16	C15	120.1(5)
C17	C16	H16	119.9
C15	C16	H16	119.9
C18	C17	C16	120.4(5)
C18	C17	H17	119.8
C16	C17	H17	119.8
C17	C18	C19	120.2(5)
C17	C18	H18	119.9
C19	C18	H18	119.9
C18	C19	C14	120.1(5)
C18	C19	H19	120.0
C14	C19	H19	120.0
C25	C20	C21	118.9(4)
C25	C20	C2	121.3(4)
C21	C20	C2	119.8(4)
C22	C21	C20	120.0(4)
C22	C21	H21	120.0
C20	C21	H21	120.0
C23	C22	C21	120.5(4)
C23	C22	H22	119.8
C21	C22	H22	119.8
C22	C23	C24	119.9(4)
C22	C23	H23	120.1
C24	C23	H23	120.1
C23	C24	C25	120.8(4)
C23	C24	H24	119.6

C25	C24	H24	119.6
C24	C25	C20	119.9(4)
C24	C25	H25	120.0
C20	C25	H25	120.0
C2	O1	C1	121.4(3)
C13	O2	H2O	109.5
O4	N1	O5	121.5(5)
O4	N1	O3	119.0(5)
O5	N1	O3	119.5(5)

Compound **1**(BF₄) crystallizes in the triclinic space group *P*-1 and the asymmetric unit is composed by one molecule of **1** ion and one BF₄⁻ counterion (see figure SI-15).

1 ion shows coplanarity between the pyrylium, the hydroxystyryl group and one phenyl ring: the relative dihedral angle are 4.81° and 3.86°. The remaining phenyl ring forms a dihedral angle of 18.61° with the pyrylium group.

The hydroxyl group acts as H-donor towards the BF₄⁻ counterion and originates a single O-H···F H-bond. Further C-H···F H-bonds can be observed at the solid state: in particular the H-donor C-H groups are both aromatic and olefinic carbons of the ligand moiety. The H-bond motif originates the supramolecular dimer shown in figure SI-16. Geometrical features of the H-bond are reported in table SI-6. Selected bond distances and angles are shown in tables SI-7, SI-8 and SI-9.

Also in this case the flat aromatic groups favor the creation of face-to-face π-interactions originating π-stacked columns of molecules (figure SI-17). The shortest centroid-centroid distance occurs between the pyrylium ring and the phenyl ring of an overlying **1** moiety. Longer distance occurs between pyrylium ring and the phenolic ring of an underlying **1** ion. The not-coplanar phenyl ring is not involved in supramolecular π-interactions.

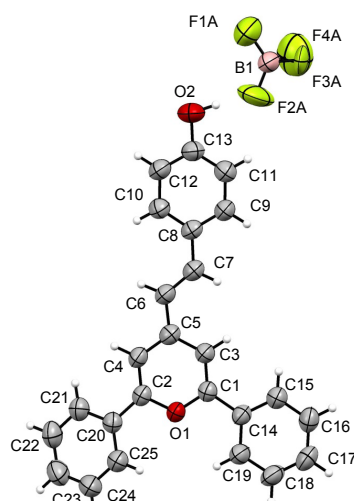


Figure SI-15. ORTEP view of the complex **1**(BF₄) (ellipsoids are drawn at the 50% probability level)

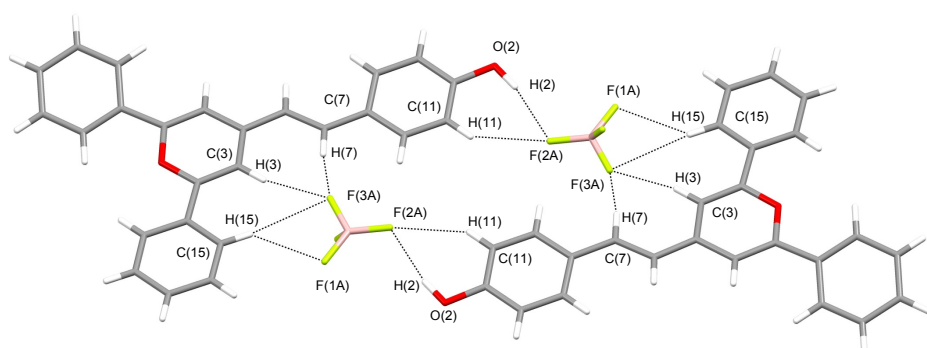


Figure SI-16. A simplified view of the H-bond dimer occurring in the crystal of **1**(BF₄)

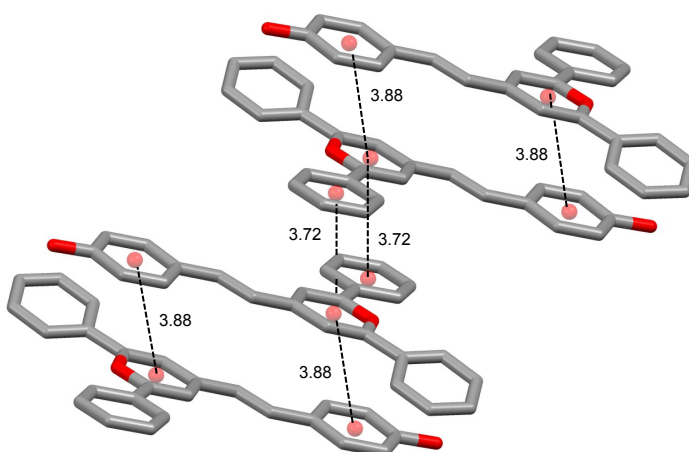


Figure SI-17. A simplified view of the π -stacked molecules occurring in the crystal of **1(BF₄)**

Table SI-6. Geometrical features for hydrogen bonds in **1(BF₄)**

Donor group (D)	D···A (Å)	H···A (Å)	D-H···A (°)	acceptor atom(A)
O(2)-H(2O)	2.860(1)	1.971(1)	154.41(1)	F(2A) _{BF4-}
C(11)-H(11C)	3.238(1)	2.575(1)	128.63(1)	F(2A) _{BF4-}
C(15)-H(15C)	3.336(1)	2.634(1)	132.73(1)	F(1A) _{BF4-}
C(15)-H(15C)	3.585(1)	2.663(1)	171.44(1)	F(3A) _{BF4-}
C(3)-H(3C)	3.406(1)	2.499(1)	164.92(1)	F(3A) _{BF4-}
C(7)-H(7C)	3.310(1)	2.438(1)	155.92(1)	F(3A) _{BF4-}

Table SI-7. π - π bonds distance (Å) for **1(BF₄)**

donor (D)	D···A
C(1)-C(15)	3.448
O(1)-C(15)	3.716
C(3)-C(15)	3.724
C(3)-C(14)	3.744
C(3)-C(19)	3.668
C(5)-C(18)	3.692
C(5)-C(17)	3.347
C(5)-C(16)	3.650
C(4)-C(16)	3.728
C(2)-C(16)	3.795
Centroid O(1)-C(5)—centroid C(14)-C(19)	3.713

Table SI-8. Distances bond (Å) for **1(BF₄)**

C1	O1	1.355(3)
C1	C3	1.360(3)
C1	C14	1.466(3)
C2	O1	1.350(3)
C2	C4	1.360(3)
C2	C20	1.460(3)
C3	C5	1.405(3)
C3	H3	0.9300
C4	C5	1.406(3)
C4	H4	0.9300
C5	C6	1.437(3)
C6	C7	1.343(4)
C6	H6	0.9300

C7	C8	1.442(3)
C7	H7	0.9300
C8	C10	1.389(3)
C8	C9	1.392(4)
C9	C11	1.372(4)
C9	H9	0.9300
C10	C12	1.371(4)
C10	H10	0.9300
C11	C13	1.372(4)
C11	H11	0.9300
C12	C13	1.379(4)
C12	H12	0.9300
C13	O2	1.353(3)
C14	C19	1.387(3)
C14	C15	1.395(3)
C15	C16	1.373(4)
C15	H15	0.9300
C16	C17	1.368(4)
C16	H16	0.9300
C17	C18	1.372(4)
C17	H17	0.9300
C18	C19	1.375(4)
C18	H18	0.9300
C19	H19	0.9300
C20	C25	1.382(4)
C20	C21	1.394(4)
C21	C22	1.373(4)
C21	H21	0.9300
C22	C23	1.370(4)
C22	H22	0.9300
C23	C24	1.368(4)
C23	H23	0.9300
C24	C25	1.380(4)
C24	H24	0.9300
C25	H25	0.9300
O2	H2O	0.949(10)
B1	F3A	1.231(8)
B1	F2A	1.270(8)
B1	F3B	1.300(10)
B1	F1A	1.313(4)
B1	F2B	1.353(8)
B1	F4B	1.404(12)
B1	F4A	1.432(8)
F2A	F4B	1.022(16)
F2A	F2B	1.282(13)
F3A	F3B	0.61(2)
F3A	F4A	1.564(13)
F4A	F2B	1.455(10)

Table SI-9. Angles for **1(BF₄)**

O1	C1	C3	119.7(2)
O1	C1	C14	112.9(2)
C3	C1	C14	127.5(2)
O1	C2	C4	119.8(2)
O1	C2	C20	112.7(2)
C4	C2	C20	127.4(2)
C1	C3	C5	120.9(2)
C1	C3	H3	119.6
C5	C3	H3	119.6
C2	C4	C5	120.8(2)

C2	C4	H4	119.6
C5	C4	H4	119.6
C3	C5	C4	116.9(2)
C3	C5	C6	123.3(2)
C4	C5	C6	119.8(2)
C7	C6	C5	124.3(2)
C7	C6	H6	117.9
C5	C6	H6	117.9
C6	C7	C8	128.1(2)
C6	C7	H7	116.0
C8	C7	H7	116.0
C10	C8	C9	117.4(2)
C10	C8	C7	123.9(2)
C9	C8	C7	118.8(2)
C11	C9	C8	121.7(2)
C11	C9	H9	119.2
C8	C9	H9	119.2
C12	C10	C8	121.2(3)
C12	C10	H10	119.4
C8	C10	H10	119.4
C9	C11	C13	119.7(3)
C9	C11	H11	120.1
C13	C11	H11	120.1
C10	C12	C13	120.1(3)
C10	C12	H12	119.9
C13	C12	H12	119.9
O2	C13	C11	123.1(3)
O2	C13	C12	117.0(3)
C11	C13	C12	119.9(3)
C19	C14	C15	118.7(2)
C19	C14	C1	121.5(2)
C15	C14	C1	119.9(2)
C16	C15	C14	120.2(3)
C16	C15	H15	119.9
C14	C15	H15	119.9
C17	C16	C15	120.6(3)
C17	C16	H16	119.7
C15	C16	H16	119.7
C16	C17	C18	119.7(3)
C16	C17	H17	120.2
C18	C17	H17	120.2
C17	C18	C19	120.7(3)
C17	C18	H18	119.6
C19	C18	H18	119.6
C18	C19	C14	120.1(3)
C18	C19	H19	120.0
C14	C19	H19	120.0
C25	C20	C21	119.3(2)
C25	C20	C2	121.3(2)
C21	C20	C2	119.3(2)
C22	C21	C20	119.9(3)
C22	C21	H21	120.1
C20	C21	H21	120.1
C23	C22	C21	120.5(3)
C23	C22	H22	119.8
C21	C22	H22	119.8
C24	C23	C22	120.1(3)
C24	C23	H23	120.0
C22	C23	H23	120.0
C23	C24	C25	120.4(3)

C23	C24	H24	119.8
C25	C24	H24	119.8
C24	C25	C20	119.9(3)
C24	C25	H25	120.1
C20	C25	H25	120.1
C2	O1	C1	121.82(19)
C13	O2	H2O	106(2)
F3A	B1	F2A	114.6(7)
F3A	B1	F3B	27.9(9)
F2A	B1	F3B	108.7(9)
F3A	B1	F1A	118.8(5)
F2A	B1	F1A	123.8(6)
F3B	B1	F1A	110.0(7)
F3A	B1	F2B	122.2(8)
F2A	B1	F2B	58.4(6)
F3B	B1	F2B	144.6(8)
F1A	B1	F2B	103.4(6)
F3A	B1	F4B	112.1(9)
F2A	B1	F4B	44.6(7)
F3B	B1	F4B	88.6(10)
F1A	B1	F4B	97.9(6)
F2B	B1	F4B	98.0(7)
F3A	B1	F4A	71.5(6)
F2A	B1	F4A	111.5(9)
F3B	B1	F4A	99.0(7)
F1A	B1	F4A	100.7(5)
F2B	B1	F4A	62.9(5)
F4B	B1	F4A	155.9(7)
F4B	F2A	B1	74.6(9)
F4B	F2A	F2B	128.8(15)
B1	F2A	F2B	64.0(6)
F3B	F3A	B1	82.3(13)
F3B	F3A	F4A	141.5(15)
B1	F3A	F4A	60.3(6)
B1	F4A	F2B	55.9(4)
B1	F4A	F3A	48.3(4)
F2B	F4A	F3A	97.0(6)
F2A	F2B	B1	57.5(5)
F2A	F2B	F4A	109.4(8)
B1	F2B	F4A	61.2(5)
F3A	F3B	B1	69.8(15)
F2A	F4B	B1	60.7(9)